



Improvement in the measurement error of the specific binding ratio in dopamine transporter SPECT imaging due to exclusion of the cerebrospinal fluid fraction using the threshold of voxel RI count

Sunao Mizumura¹ · Kazuhiro Nishikawa² · Akihiro Murata² · Kosei Yoshimura² · Nobutomo Ishii³ · Tadashi Kokubo³ · Miyako Morooka¹ · Akiko Kajiyama¹ · Atsuro Terahara¹

Received: 22 January 2018 / Accepted: 4 March 2018 / Published online: 15 March 2018
© The Japanese Society of Nuclear Medicine 2018

Abstract

Objective In Japan, the Southampton method for dopamine transporter (DAT) SPECT is widely used to quantitatively evaluate striatal radioactivity. The specific binding ratio (SBR) is the ratio of specific to non-specific binding observed after placing pentagonal striatal voxels of interest (VOIs) as references. Although the method can reduce the partial volume effect, the SBR may fluctuate due to the presence of low-count areas of cerebrospinal fluid (CSF), caused by brain atrophy, in the striatal VOIs. We examined the effect of the exclusion of low-count VOIs on SBR measurement.

Methods We retrospectively reviewed DAT imaging of 36 patients with parkinsonian syndromes performed after injection of ¹²³I-FP-CIT. SPECT data were reconstructed using three conditions. We defined the CSF area in each SPECT image after segmenting the brain tissues. A merged image of gray and white matter images was constructed from each patient's magnetic resonance imaging (MRI) to create an idealized brain image that excluded the CSF fraction (MRI-mask method). We calculated the SBR and asymmetric index (AI) in the MRI-mask method for each reconstruction condition. We then calculated the mean and standard deviation (SD) of voxel RI counts in the reference VOI without the striatal VOIs in each image, and determined the SBR by excluding the low-count pixels (threshold method) using five thresholds: mean-0.0SD, mean-0.5SD, mean-1.0SD, mean-1.5SD, and mean-2.0SD. We also calculated the AIs from the SBRs measured using the threshold method. We examined the correlation among the SBRs of the threshold method, between the uncorrected SBRs and the SBRs of the MRI-mask method, and between the uncorrected AIs and the AIs of the MRI-mask method.

Results The intraclass correlation coefficient indicated an extremely high correlation among the SBRs and among the AIs of the MRI-mask and threshold methods at thresholds between mean-2.0SD and mean-1.0SD, regardless of the reconstruction correction. The differences among the SBRs and the AIs of the two methods were smallest at thresholds between mean-2.0SD and mean-1.0SD.

Conclusion The SBR calculated using the threshold method was highly correlated with the MRI-SBR. These results suggest that the CSF correction of the threshold method is effective for the calculation of idealized SBR and AI values.

Keywords ¹²³I-FP-CIT · Dopamine transporter SPECT · Southampton method · Threshold · Cerebrospinal fluid · Striatum binding ratio

Introduction

Dopamine transporter (DAT) single-photon emission tomography (SPECT) is an effective imaging modality for the diagnosis of parkinsonian syndrome, including Parkinson's disease and Dementia with Lewy body [1, 2]. While a visual approach is generally accepted, and is often the preferred method for analysis of DAT scans, it is difficult to visually interpret some cases of subtle or symmetrical decreases of radioactivity in the striata that require the quantitative

✉ Sunao Mizumura
sunaom@med.toho-u.ac.jp

¹ Department of Radiology, Toho University Omori Medical Center, 1-1-5, Omori-nishi, Ota-ku, Tokyo 143-8541, Japan

² Nihon Medi-Physics Co., Ltd., 3-4-10, Shinsuna, Koto-ku, Tokyo 136-0075, Japan

³ Central Radiology Division, Toho University Omori Medical Center, Omori-nisho, Ota-ku, Tokyo, Japan

evaluation of nigrostriatal dopamine function. Most semi-quantitative analysis in positron emission tomography (PET) studies uses binding ratios that calculate the accumulation ratio of the striatum to the reference area, which indicates non-specific binding (cerebellar or occipital cortex) [3–7]. However, in DAT SPECT studies, it is difficult to place the voxel of interest (VOI) in the cerebellar or occipital cortex because those areas are invisible in many DAT SPECT images. It is also difficult to trace a striatum with low radioactivity.

Large geometric VOIs are used to circumvent the problems in DAT SPECT images; quadrangular or pentagonal prism VOIs are used to cover the striata, and elliptic cylinder VOIs except striatum VOIs are used to calculate whole brain non-specific binding [8–10]. DaTView software (Hayabusa, AZE Co., Ltd., Tokyo, Japan) is a semiautomatic processor used for the semi-quantitative analysis proposed by Tossi-Bolt et al. (Southampton method) [8, 9], and is used at many institutions in Japan. In the Southampton method, the radioactivity in a striatal VOI consists of the activity in each striatum (reflecting specific binding), the activity in structures except the striatum (reflecting non-specific binding), and the activity in cerebrospinal fluid (CSF) in cerebral fissures and ventricles, which has little radioactive scatter. The radioactivity in the reference VOI includes the activity of the whole brain except the striatum VOI (reflecting non-specific binding) and the CSF (Fig. 1).

However, underestimation of specific and non-specific binding in an atrophic brain is inevitable due to the enlargement of the cerebral ventricle or cerebral fissure. The specific binding ratio (SBR) is calculated using the Southampton method, as follows:

$$\text{SBR} = \frac{T/\text{CR} - V}{\text{VS}}, \quad (1)$$

where T is the total activity in the striatal VOI, VS is the volume of the striatum (assumed to be 11.2 ml), V is the volume of the striatal VOI, and CR is the ^{123}I -FP-CIT activity concentration in the reference region.

The method is vulnerable to contamination by CSF due to atrophy, and fluctuates according to the distribution of the atrophied regions. Therefore, accurate SBR calculation requires exclusion of the CSF in fissures and ventricles from the striatal and reference VOIs. We made a mask image of each SPECT image to determine the idealized SBR. An individual MRI image, to which the SPECT image is coregistered, is segmented into three images: gray matter, white matter, and the CSF image. The mask image is created by merging the gray and white matter areas after segmentation. We obtained an accurate SBR independent of the CSF area if the SBR was calculated using masked-out SPECT images (MRI-mask method). However, this masking procedure is tedious, time-consuming, and highly operator-dependent, and is not suitable for clinical use.

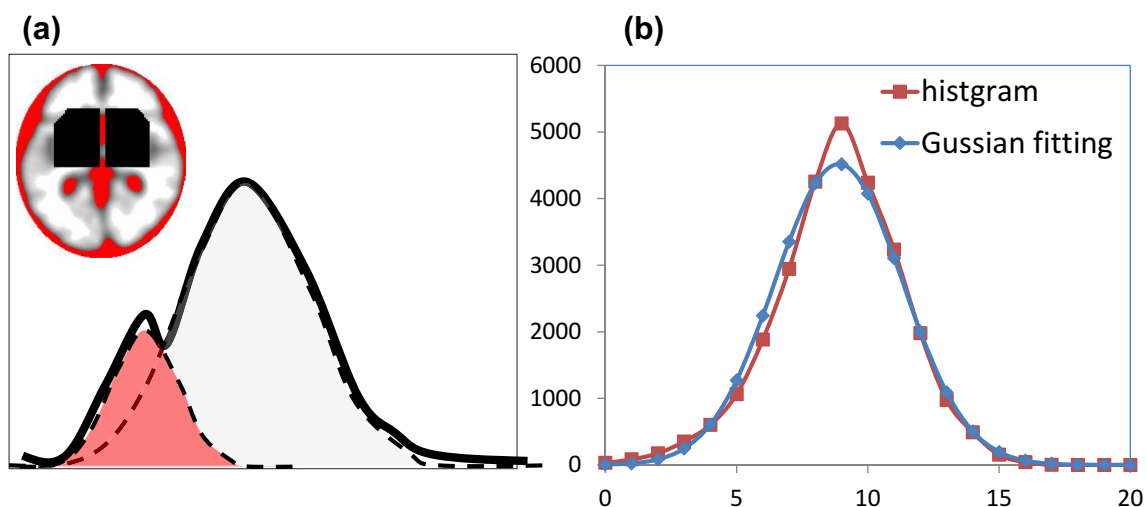


Fig. 1 Histogram of voxel RI counts in the whole brain except striatal VOI. **a** Schematic diagram of the histogram of RI counts of the whole brain VOI except the striatal VOIs. The red areas of the histogram and tomographic image are the cerebrospinal fluid (CSF) fraction. The histogram is assumed to include two single-peak curves that consist of non-specific binding (gray matter and white matter fractions) and the scattering counts (CSF fraction). **b** Histogram of RI counts of the whole brain VOI except the striatal VOI. The single peak is the approximate standardized distribution by Gaussian conversion.

It shows the accumulation merged with the non-specific binding and CSF areas. The non-specific binding fraction was determined by extracting the lower RI count voxels with scatter in the CSF area from the area under the single-peak curve. (The CSF fraction is much smaller than the whole brain fraction, and its accumulation is near to the accumulation of the whole brain fraction. The actual CSF fraction, unlike the schema, is not separate from the whole brain fraction. Then, the summated curve of two fractions may slightly shift left from the gamma fitting curve.)

In this study, we postulated that the accumulation of CSF would be the lowest in the striatal and reference VOIs, because the accumulation of CSF in striatal and reference VOIs consists of only the scattering radioactive fraction. We expect that SBR measurement error due to brain atrophy can be reduced by excluding the lowest activity areas from the SBR calculation. For example, after calculating the mean and standard deviation (SD) of the reference VOI using Gaussian fitting of the counts (entire brain area except striatal VOIs), we defined the threshold of non-specific binding from the mean and SD. We then evaluated the accuracy of the SBR using the counts of the striatal and reference VOIs that were above the threshold (threshold method). Finally, we compared the SBR of the threshold method with that of the morphological MRI-mask method regarded as the idealized SBR without the CSF fraction. We also calculated and compared the asymmetric index (AI) of the SBR of the threshold method with that of the MRI-mask method. It is important to estimate the differences in accumulation in the striata that are associated with the motor-symptom laterality of parkinsonian syndrome. We tested the correction of the exclusion of CSF artifacts for the accurate calculation of the SBR and AI of nigrostriatal dopamine function.

Materials and methods

Patients

Thirty-six patients (9 males and 27 females; mean age, 70.6 ± 10.4 years; range, 41–90 years) with suspected parkinsonian syndrome (PS) were enrolled in this study. The clinical diagnosis of each patient was PS or non-PS; healthy control subjects were included. Each patient was injected with ^{123}I -*N*-*x*-fluoropropyl-2 β -carbo-methoxy-3 β -(4-iodophenyl)nortropan (^{123}I -FP-CIT), and a three-dimensional T1W1 sagittal MR image of each patient was acquired. The range of SBR with attenuation correction (AC) and without scatter correction (no SC) was 0.58–5.22; the mean was 3.17. The retrospective study was done in accordance with the current revision of the Declaration of Helsinki and Good Clinical Practice, and was approved by the Ethical Review Board of the Medical Centre Omori, Toho University.

Acquisition and reconstruction

DAT SPECT

Each patient ($n = 36$) was injected with approximately 167 MBq of ^{123}I -FP-CIT and remained in a quiet, supine position for 30 min, after which an image was acquired. Images of 26 of the 36 patients were collected using a triple head GCA-9300R SPECT camera (Canon Medical Systems

Co., Ltd., Tokyo, Japan) with Low-Medium Energy General Purpose (LMEGP) fan-beam (N2) collimators. Ninety projection images were obtained from 5 rotation data in 360° by each 120° head as 4° per step $\times 30$ steps; each step required 12 s, and the radius of rotation was minimized for each subject. The matrix size was 128×128 ; the magnification factor of 1.00 resulted in a pixel size of 1.72 mm. Counts were acquired within a 30% symmetrical energy window centered at 159 keV. Images of the other 10 patients were collected using a dual head Infinia SPECT camera (GE Healthcare Japan Co., Ltd., Tokyo, Japan) with a step-and-shoot mode. Sixty projection images were obtained in 360° by each 180° head as 6° per step $\times 30$ steps; each step required 60 s, and the radius of rotation was minimized for each subject. The matrix size was 128×128 and the magnification factor was 1.50. Counts were acquired within a 20% symmetrical energy window centered at 159 keV.

Data were reconstructed using filtered back-projection with a Butterworth filter (GCA-9300R: order 4, cut-off frequency 0.65 cycles/cm; Infinia: order 10, cut-off frequency 0.60 cycles/cm). The Chang method was used for AC: $\mu = 0.070 \text{ cm}^{-1}$ in non-SC and $\mu = 0.146 \text{ cm}^{-1}$ in SC. The triple energy window (TEW) method (sub window 7%) of SC was used [11]. To examine the differences among the correction methods due to CSF mask correction, the images were reconstructed using three reconstruction conditions: “AC + SC+,” “AC + SC-,” and “AC–SC-.”

MR imaging

Images were acquired using a 1.5T Toshiba EXCELART™ Vantage scanner (Canon Medical Systems). Initially, a sagittal T1-weighted field echo sequence (TE = 14 ms, TR = 500 ms, field of view = 240 mm, slice thickness = 6 mm with 0.6-mm gaps, 15 slices) was acquired to confirm the presence of brain atrophy and to discard any signs of infarction or other lesions in the subjects. Subsequently, a series of contiguous coronal images 2 mm thick across the entire brain was acquired using a T1-weighted fast field echo sequence (TE = 5.5 ms, TR = 24.4 ms, flip angle = 35° , field of view = 240 mm, 256×256 matrix). Slices were positioned along the anterior commissure–posterior commissure (AC–PC) line.

Image processing and assessment

SBR and Asymmetry Index (AI) of the MRI-mask method

Figure 2b shows the process of the creation of a masked SPECT image of morphological exclusion of CSF using segmented MRI. To validate the CSF correction effect by removing the low-count areas of an atrophic brain, three-dimensional (3D) MRI images were segmented into gray

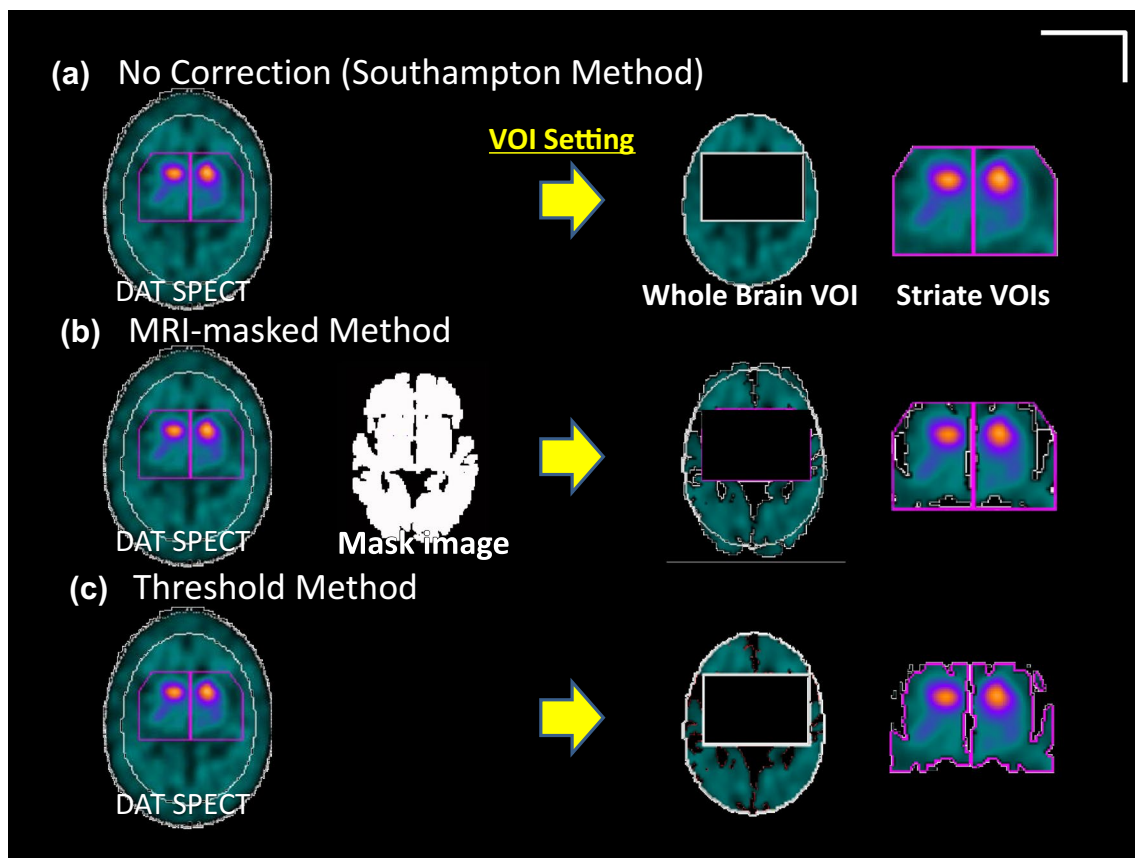


Fig. 2 Methods of measurement of the specific binding ratio. **a** Southampton method. After defining the whole brain VOI and the contour of the bones of the skull, non-specific binding was defined as the average count in the whole brain except the pentagonal striata VOIs. Specific binding was measured as the average counts in the pentagonal striata VOIs. The SBR was calculated from the ratio of the average counts. **b** MRI-mask method. An MRI mask image was created from the sum of the gray and white matter images to which the 3D-MRI image was segmented. The SPECT image, coregistered to MRI, was preserved with the mask image. The specific

binding ratio was calculated from the average accumulation in the striata VOIs and the whole brain, excluding the striatal VOIs in the reserved SPECT image. **c** Threshold method. Based on the assumption that there is a CSF fraction in the area of lowest activity of the whole brain VOI, the threshold between non-specific binding and the CSF was set using the mean and SD of a Gaussian-fitted histogram of whole brain VOI counts. The specific binding ratio was calculated using the average accumulation after excluding the areas in the striata and whole brain VOIs that were below the threshold

matter, white matter, and CSF images after transaxial images horizontal to the AC–PC line were taken using SPM8 (Statistical Parametric Mapping, <http://www.fil.ion.ucl.ac.uk/spm>) [12–14]. The mask image was defined as the extracted pixels by thresholding more than 50% of the average signal intensity in the MRI merge of the gray and white matter images.

Subsequently, the DAT SPECT imaging was coregistered to 3D MRI and filtered through the mask image. The SBR was calculated from the masked SPECT image using the Southampton method (MRI–SBR) and was considered the idealized SBR, as it canceled the CSF fraction. As an indicator of radioactive laterality, the AI of the DaTView software was defined as follows:

$$AI = \frac{|(\text{SBR of left striatum}) - (\text{SBR of right striatum})|}{(\text{SBR of left striatum}) + (\text{SBR of right striatum})} \times 100\% . \quad (2)$$

The AI obtained using the MRI-mask images was defined as the MRI–AI.

SBR and AI of the threshold method, excluding the low-count fraction

DAT SPECT images were transformed horizontally into the AC–PC plane using software (BrainObliqu, Hayabusa, AZE Co., Ltd., Tokyo, Japan) to reconstruct the oblique image from the SPECT scans. Those oblique images were coregistered with individual MRI images using the “coreg.exe” function of the NEUROSTAT program (Department of Internal Medicine, University of Michigan, Ann Arbor, MI, USA) [15–17]. The mean and SD were then calculated using the distribution of the counts in the reference VOI, which

were considered to have approximately Gaussian distribution on DaTView software.

Due to the different distribution of low-count areas in each patient, we defined the threshold for the exclusion of low-count areas using individual mean and SD values according to Gaussian fitting of the counts in the reference VOI. To determine a suitable threshold for accurate SBR and AI in the threshold method, we prepared five thresholds in the reference VOI: mean-0.0SD, mean-0.5SD, mean-1.0SD, mean-1.5SD, mean-2.0SD (Fig. 2c). In addition, we calculated the non-corrected SBR (equal to the SBR and AI according to the original Southampton method [uncorrected SBR and AI]). However, when the SBR of the threshold method was negative due to incomplete correction, the corresponding AI of the threshold method was not available. In one patient imaged using the GCA-9300R and in two patients imaged using the Infinia, the AIs of the threshold method data were excluded from the analysis.

Comparison of the SBRs and AIs of the MRI-mask and threshold methods

We investigated the correlations between the five obtained SD-SBRs and the SBR of the non-corrected method with the SBR of the MRI-mask method, and of the five AIs of the MRI-mask method and the AI of the non-corrected method with the AI of the MRI-mask method, respectively. Generally, a linear correlation between two parameters is used in Pearson's correlation coefficient. However, we used the intraclass correlation coefficient (ICC(1,1); $p < 0.01$) to determine the correlation between the SBRs and between the AIs. We also examined the measured error to determine the differences between the SBRs and between the AIs of the threshold and MRI-mask methods.

Results

DAT SPECT images of the threshold method

Figure 3 shows the corrected images created using the MRI-mask method and the threshold method that excluded the CSF fraction. The area under the threshold increased gradually as the threshold value increased from mean-2.0SD to mean-0.0SD (2.3–50.0% fewer total pixels were excluded from the SBR calculation as the CSF area in the reference VOI).

Comparison of the SBRs of the threshold and MRI-mask methods

Figure 4 shows the ICC(1,1) of the SD-SBRs and MRI-SBRs of each of the three reconstruction conditions. The

SBR of the threshold method was strongly concordant with the SBR of the MRI-mask method, regardless of the reconstruction conditions and threshold values for the exclusion of the CSF. However, the measurement error of the SBR was lowest at thresholds between mean-1.5SD and mean-0.5SD (6.7–30.9% fewer pixels) (Fig. 5).

Comparison of the AIs of the threshold and MRI-mask methods

A degree of concordance was observed between the AIs of the threshold and the MRI-mask methods, though the correlation between the AIs of the non-corrected and MRI-mask methods was extremely low.

However, concordance was not observed in AC–SC– images, except at thresholds between mean-2.0SD and mean-1.0SD (2.3–15.9% fewer pixels) (Fig. 6). The difference in the SBR was lower at thresholds above mean-2.0SD (2.3% fewer pixels) (Fig. 7).

Discussion

The visual assessment of DAT SPECT images is sufficiently useful for the diagnosis of early PD from the findings of radioactive laterality or low radioactivity in the posterior putamen. However, a quantitative evaluation is also required to measure the severity of the DAT reduction, both for evaluation of the relationship between the clinical symptoms and the DAT density, and for follow-up studies.

The Southampton method, widely used in Japan, can be used to determine the SBR without the partial volume effect, independent of the resolution of the SPECT image. The striatal VOIs of the Southampton method are large enough to cover each striatum, while other quantitative methods require the VOI trace on the edge of the striata. However, the SBR of the Southampton method is occasionally unstable, especially in cases of brain atrophy, which presents as CSF that permeates fissures and ventricles of striatal and reference VOIs. In this study, the CSF fraction of the striatal and reference VOIs was assumed to be the lowest accumulation. Therefore, we excluded this fraction from the image processing of the SBR calculation.

The concordance between the SBR of the threshold method and the SBR of the MRI-mask method was adequately superior to that of SBR of the Southampton method (SBR of the uncorrected image) of any reconstruction condition (such as attenuation and scattering corrections), although the SBR of the uncorrected condition was highly concordant with the SBR of the MRI-mask method, independent of the reconstruction conditions. Moreover, we examined the difference between the SBRs of the MRI-mask and threshold methods. The SBRs of the MRI-mask and

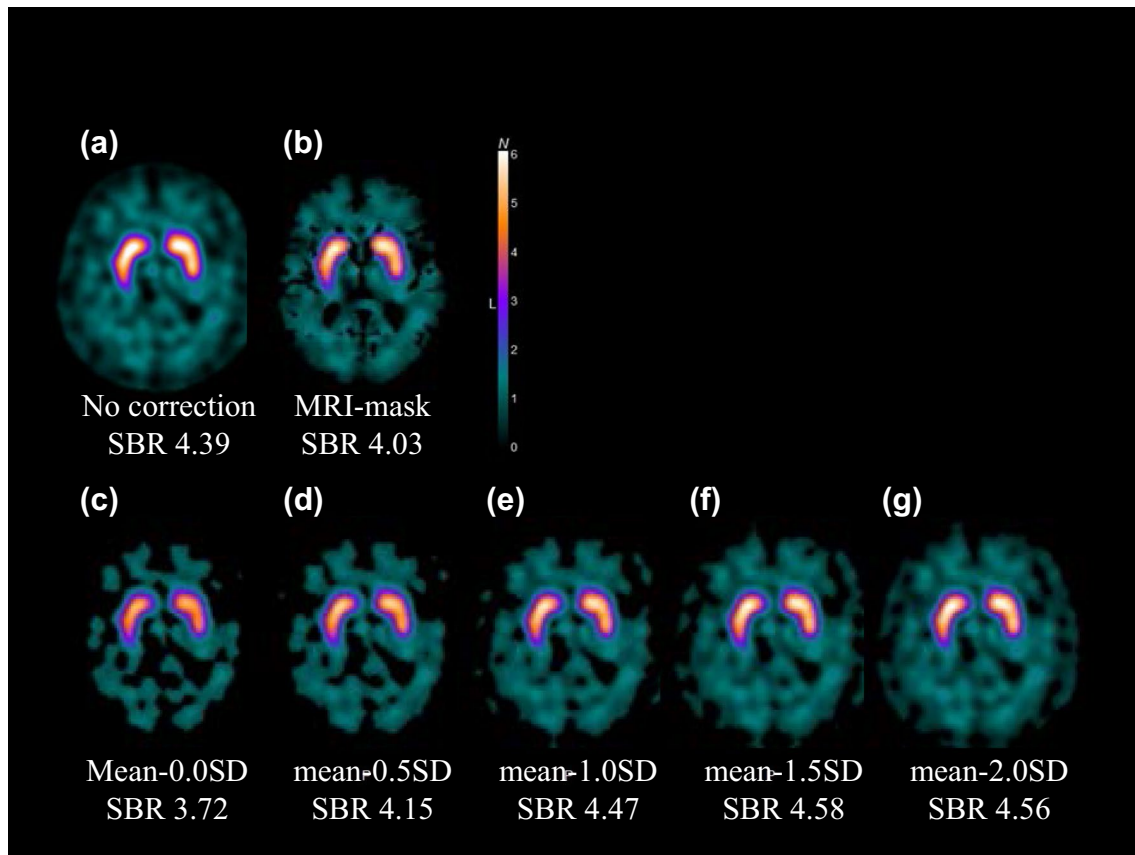


Fig. 3 SPECT images after masking and thresholding. **a** Non-corrected and **b** MRI-mask images. **c–g** Five thresholded images with cut-off values of mean-0.0SD to mean-2.0SD. Striatal uptake in the MRI-mask image is slightly higher than in the non-corrected image

due to morphometric removal of the CSF fraction. Striatal uptake on exclusion of low-count areas decreased as the threshold increased. It seems that the thresholded image with a cut-off value of mean-1.0SD is closest to the MRI-mask image

threshold methods were the lowest at thresholds of mean-0.5SD to mean-1.5SD.

However, the ICC(1,1) of the AI, which depended upon the reconstruction conditions or the SPECT camera used, was generally lower than the ICC(1,1) of the SBR. The measurement error of the SBR increases the error of the AI because the AI is calculated from the left and right SBRs.

Nevertheless, the corresponding AI with negative SBR value in some cases was excluded, and the concordance of the non-corrected AI with the AI of the MRI-mask method was lower than that of SBR of the threshold method. At least, the threshold method provides a higher reliability than the non-corrected one.

Considering the effect of the different SPECT cameras and reconstruction conditions, there was a fair concordance between the AIs of the threshold and MRI-mask methods with thresholds of mean-1.0SD to mean-2.0SD.

From these results, the correction that excluded the CSF fraction was confirmed to be more efficient than the original Southampton method. A threshold between mean-1.0SD

and mean-1.5SD was presumed to be the most effective for calculation of the SBR and AI using the threshold method.

These results suggest that setting the threshold below mean-2.0SD leaves the CSF fraction in the striatal and reference VOIs, and setting the threshold above mean-0.5SD removes the brain tissue fraction excessively, which leads to a lower concordance of SBR and AI. The border between non-specific binding and CSF would be in the threshold from mean-1.5SD to mean-1.0SD in this study. It is expected that the minor setting error of the border does not cause much SBR fluctuation in the accumulation of the reference VOI, even if the border between the two fractions was incorrectly recognized in some cases, because the non-specific binding and CSF around the border have similar accumulations.

Simple semi-quantitative methods such as the Southampton method would be used for the measurement of accurate SBRs of SPECT images with low resolution, though, as reported previously (3–7), it is preferable to place the reference VOI on the occipital cortex or cerebellum for SBR calculation. We hope to obtain comparatively accurate results in

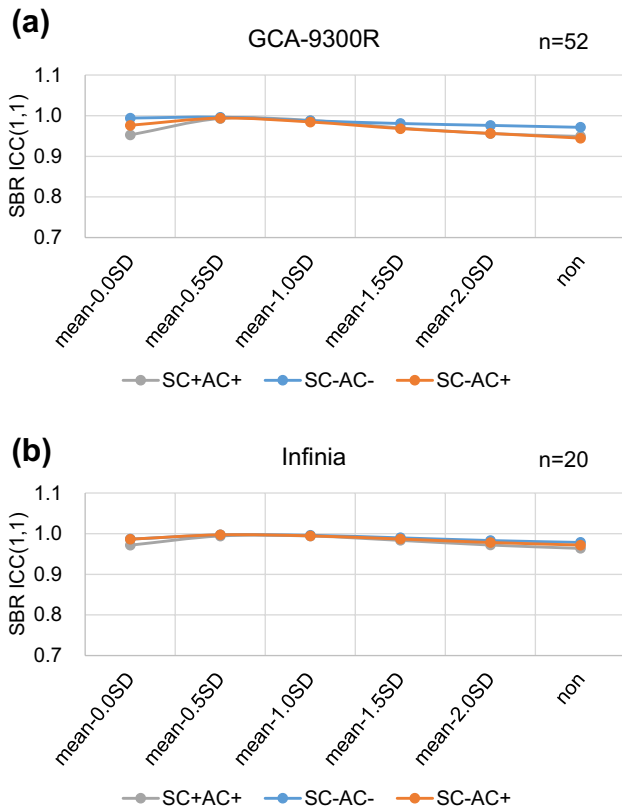


Fig. 4 Intra-class correlation coefficient of the SBR using a 3-headed GCA-9300R camera and a 2-headed Infinia camera. The ICC(1,1) of SBRs using **a** GCA-9300R and **b** Infinia cameras. This graph shows the SBR of each reconstruction condition, as follows: AC–SC–, blue line; AC+SC–, red line; AC+SC+, black line. The *x*- and *y*-axes indicate the CSF-corrected threshold and the ICC(1,1). The concordance between the SBRs of the two SPECT cameras was high

clinical applications using the approximate semi-quantitative method of SBR calculation by excluding lower-count voxels.

Limitations

The threshold method cancels low-count voxels to exclude the CSF fraction from striatal and reference VOIs using the threshold defined by the mean and SD of an approximately Gaussian fitting distribution of the histogram of the reference VOI. When the size of the reference VOI setting is much larger or much smaller, the border of the CSF fraction in the VOIs changes. This method requires a relevant trace of the outer margin of the whole brain in settings on the reference VOI.

In addition, the use of ordered subset expectation maximization (OSEM) reconstruction or strong filtering results in good uniformity in SPECT images, and may present a better coefficient of SBR in the MRI-mask and threshold methods. However, strong smoothing causes a reduction in lesion contrast, leading to lower sensitivity to local lesions.

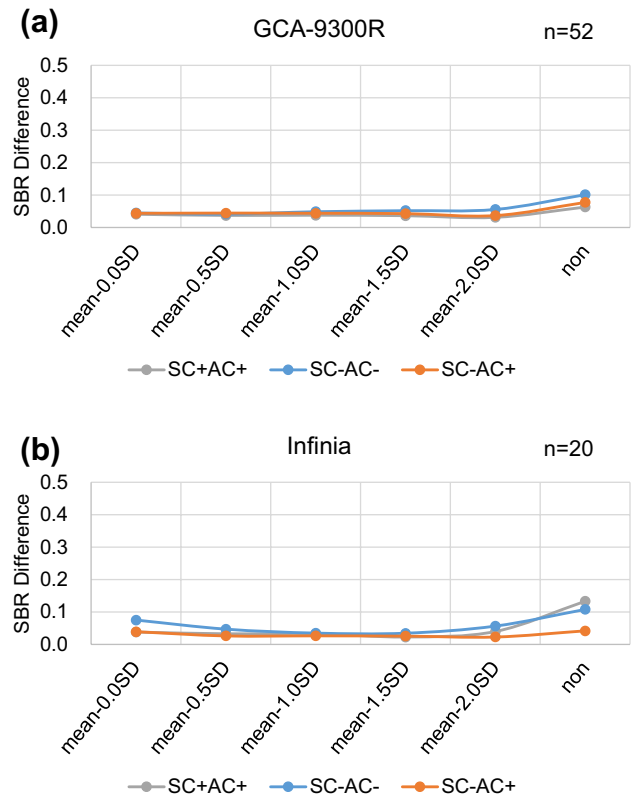


Fig. 5 Difference between the SBRs of the GCA-9300R and Infinia cameras. Differences between the SBRs of the **a** GCA-9300R and **b** Infinia cameras. This graph shows the AI value of each reconstruction condition, as follows: AC–SC–, blue line; AC+SC–, red line; AC+SC+, black line. The *x*- and *y*-axes indicate the CSF-corrected threshold and the difference between the SBRs of the MRI-mask and threshold methods. The difference in the SBR was very low for each reconstruction condition and each camera, and was much lower at threshold values of mean-0.5SD to mean-1.5SD

Therefore, a good assessment of DAT SPECT images must balance contrast and uniformity.

In this study, we verified the CSF correction effect using a limited number of SPECT cameras and under a number of limited reconstruction conditions. Future studies must validate the correction effects in additional SPECT devices using additional reconstruction conditions.

Conclusions

The SBR based on the Southampton method may be over- or underestimated due to the presence of CSF in striatal and reference VOIs in an atrophic brain. We developed a new method to exclude the CSF fraction from these VOIs by removing the low-count areas from the calculation. The SBR and AI determined using this method correlated well with those calculated using morphometric masking SPECT with MRI. This suggests that this method would improve

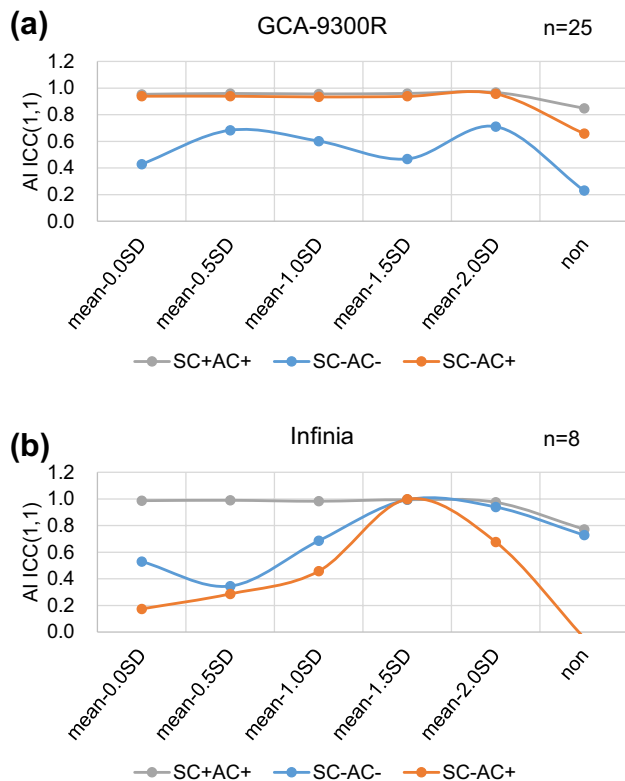


Fig. 6 Intra-class correlation coefficient (ICC(1,1)) of the AIs of the 3-headed GCA-9300R and 2-headed Infinia cameras. The ICC(1,1) of the AIs of the **a** GCA-9300R and **b** Infinia cameras. This graph shows the AI value of each reconstruction condition, as follows: AC–SC– blue line; AC+SC–, red line; and AC+SC+, black line. The x- and y-axes indicate the CSF-corrected threshold and the ICC(1,1). **a** In images reconstructed using AC+SC– and AC+SC+, the concordance between the AIs of the MRI-mask and uncorrected methods was high. However, the concordance between the AI of the uncorrected method was not necessarily equal to that of the MRI-mask method because some cases had a negative SBR if not corrected. **b** The concordance of the SBR was high in the AC+SC+ condition. At threshold values of mean-1.0SD to mean-2.0SD, the AIs of the MRI-mask are concordant to those of MRI-mask method, even in AC+SC– and AC–SC– conditions

the accuracy of the quantitative estimation of DAT SPECT in clinical use.

Compliance with ethical standards

Conflict of interest KN and AM are employees of Nihon Medi-Physics Co., Ltd. All other authors declare that they have no conflicts of interest.

References

1. Cummings JL, Henchcliffe C, Schaier S, Simuni T, Waxman A, Kemp P. The role of dopaminergic imaging in patients with

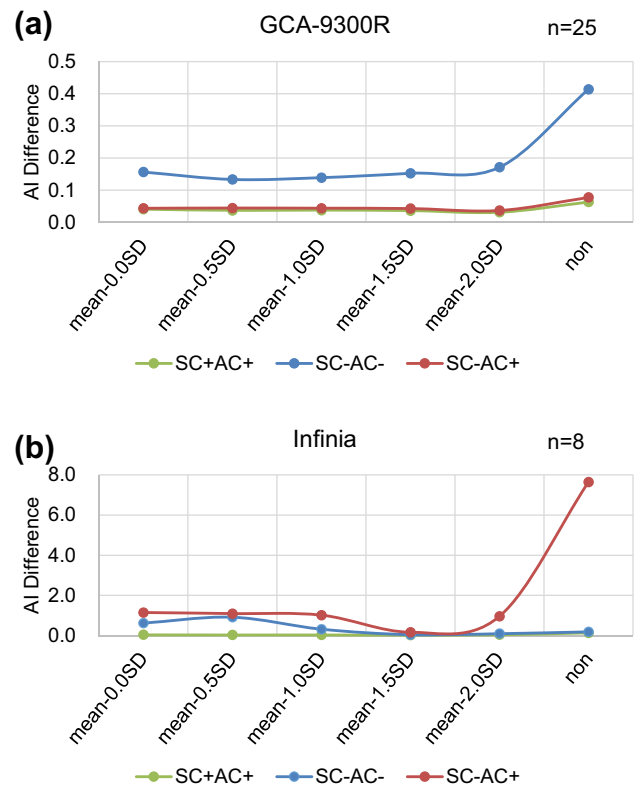


Fig. 7 Difference between the AIs of the GCA-9300R and Infinia cameras. Differences between AIs of the **a** GCA-9300R and **b** Infinia cameras. This graph shows the AI value of each reconstruction condition, as follows: AC–SC–, blue line; AC+SC–, red line; and AC+SC+, black line. The x- and y-axes indicate the setting and the CSF correction threshold, respectively. With the threshold above mean-2.0SD, the difference between the AIs of the MRI-mask and threshold methods was smaller than with any reconstruction condition

symptoms of dopaminergic system neurodegeneration. *Brain*. 2011;134(Pt 11):3146–66.

2. Tatsch K, Poepperl G. Nigrostriatal dopamine terminal imaging with dopamine transporter SPECT: an update. *J Nucl Med*. 2013;54(8):1331–8.
3. Habraken JB, Booij J, Slomka P, Sokole EB, van Royen EA. Quantification and visualization of defects of the functional dopaminergic system using an automatic algorithm. *J Nucl Med*. 1999;40(7):1091–7.
4. Takikawa S, Dhawan V, Chaly T, Robeson W, Dahl R, Zanzi I, et al. Input functions for 6-[fluorine-18] fluorodopa quantitation in parkinsonism: comparative studies and clinical correlations. *J Nucl Med*. 1994;35:955–63.
5. Dhawan V, Ma Y, Pillai V, Spetsieris P, Chaly T, Belakhlef A, et al. Comparative analysis of striatal FDOPA uptake in Parkinson's disease: ratio method versus graphical approach. *J Nucl Med*. 2002;43:1324–30.
6. Jokinen P, Helenius H, Rauhala E, Brućk A, Eskola O, Rinne JO. Simple ratio analysis of ¹⁸F-fluorodopa uptake in striatal subregions separates patients with early Parkinson disease from healthy controls. *J Nucl Med*. 2009;50:893–9.
7. Joutsa J, Johansson J, Kaasinen V. Is occipital cortex a valid reference region in ¹²³I-FP-CIT SPECT imaging? *Clin Nucl Med*. 2015;40:615–6.

8. Tossici-Bolt L, Hoffmann SM, Kemp PM, Mehta RL, Fleming JS. Quantification of [^{123}I]FP-CIT SPECT brain images: an accurate technique for measurement of the specific binding ratio. *Eur J Nucl Med Mol Imaging*. 2006;33(12):1491–9.
9. Tossici-Bolt L, Dickson JC, Sera T, de Nijs R, Bagnara MC, Jons-son C, Scheepers E, Zito F, Seese A, Koulibaly PM, Kapucu OL, Koole M, Raith M, George J, Lonsdale MN, Münzing W, Tatsch K, Varrone A. Calibration of gamma camera systems for a multi-centre European ^{123}I -FP-CIT SPECT normal database. *Eur J Nucl Med Mol Imaging*. 2011;38(8):1529–40.
10. Buchert R, Kluge A, Tossici-Bolt L, Dickson J, Bronzel M, Lange C, Asenbaum S, Booi J, Atay Kapucu L, Svarer C, Koulibaly Pobili F, Pagani M, Sabri O, Sera T, Tatsch K, Vander Borgh T, Van Laere K, Varrone A, Iida H. Reduction in camera-specific variability in [^{123}I] FP-CIT SPECT outcome measures by image reconstruction optimized for multisite settings: impact on age-dependence of the specific binding ratio in the ENC-DAT database of healthy controls. *Eur J Nucl Med Mol Imaging*. 2016;43(7):1323–36.
11. Ichihara T, Ogawa K, Motomura N, Kubo A, Hashimoto S. Compton scatter compensation using the triple-energy window method for single- and dual-isotope SPECT. *J Nucl Med*. 1993;34(12):2216–21.
12. Penny WD, Friston KJ, Ashburner JT, Kiebel SJ, Nichols TE. *Statistical mapping: the analysis of functional brain imaging*, 1st edn. 2006; Academic Press.
13. Ashburner J. A fast diffeomorphic image registration algorithm. *NeuroImage*. 2007;38(1):95–113.
14. Ashburner J, Friston K. Computing average shaped tissue probability templates. *NeuroImage*. 2009;45(2):333–41.
15. Minoshima S, Berger KL, Lee KS, Mintun MA. An automated method for rotational correction and centering of three-dimensional functional brain images. *J Nucl Med*. 1992;33:1579 – 1585.
16. Minoshima S, Koeppe RA, Mintun MA, et al. Automated detection of the intercommissural line for stereotactic localization of functional brain images. *J Nucl Med*. 1993;34:322–9.
17. Minoshima S, Koeppe RA, Frey KA, Kuhl DE. Anatomical standardization: linear scaling and nonlinear warping of functional brain images. *J Nucl Med*. 1994;35:1528 – 1537.